Sustainable Energy & Fuels

ROYAL SOCIETY OF CHEMISTRY

PAPER

View Article Online
View Journal | View Issue

Cite this: *Sustainable Energy Fuels*, 2025, **9**, 2805

Co-modification of NCM-622 *via* Mg^{2+} *in situ* doping and $LiBO_2/B_2O_3$ surface coating: a pathway to design high-voltage cathodes for lithium-ion batteries†

Praneash Venkatachalam,[ab] Kamala Kumari Duru,[f] Sambasivam Sangaraju,[c] Asha Anish Madhavan,[d] Pilgun Oh,[gh] Pardha Saradhi Maram[*be] and Sujith Kalluri[*ab]

NCM-622 cathodes have been promising cathodes for lithium-ion batteries due to their high reversible specific capacity and low cost. However, the NCM-622 cathode suffers from structural instability, especially at high voltage. Moreover, at elevated voltages and temperatures the cathode suffers from surface side reactions and particle cracks due to the presence of grain boundaries. The *in situ* doping of Mg^{2+} is achieved by doping Mg ions during the synthesis procedure using a CSTR and the $LiBO_2/B_2O_3$ surface coating is achieved by a simple wet-chemistry method; this dual-modification not only protects the surface of the cathode but the Mg^{2+} ions in the structure also enhance the cycling stability even at high voltage (4.5 V) and temperature (55 °C). As a result, animproved electrochemical behaviour was observed and the cathode could retain 82.5% of its initial capacity after 100 cycles at 4.5 V. Furthermore, the presence of the hybrid coating on the surface protects the cathode from HF attack and reduces the voltage polarisation during high temperature and voltage cycling. Such a dual-modification strategy can be commercially viable and useful for modification of high-energy-density NCM-622 cathodes.

Received 19th September 2024
Accepted 8th April 2025

DOI: 10.1039/d4se01297f

rsc.li/sustainable-energy

Introduction

Carbon emissions from Internal Combustion Engines (ICE) worldwide are a rising concern because of climatic change due to global warming. With more than 100 companies worldwide pledged to neutralise the carbon emissions from ICE vehicles and replace them with Electric and Hybrid Electric Vehicles (EV & HEV), highly efficient energy storage devices are needed.[1–3] Lithium-ion batteries (LIBs) have dominated the market for almost 20 years as highly efficient battery systems, from low-voltage consumer appliances to high-voltage electric vehicles. But with the rise in demand and more companies interested in developing EVs & HEVs, there is an imperative need for robust and highly efficient LIBs. Over the years, numerous research studies have been carried out in developing high-capacity anodes, conductive electrolytes with additives, and high-voltage cathodes.[4,5] Cathodes play a vital role in increasing the battery's voltage, and the necessity to develop such cathodes is of utmost importance. The limited voltage output of common cathode materials can act as a constraint when aiming for higher energy density in batteries. So, the need to operate the battery at higher voltages is currently a hotspot in research on LIBs.[6,7] With various cathode materials available, Ni-rich cathodes have been an attractive option for developing high-energy batteries due to their high specific capacity, moderate resources, and low cost. The increase in Ni content in the cathode has been systematically studied over the years and the role of doping ions such as Co and Mn has also been systematically investigated over the years before commercialization.[8,9] Even with all the better prospects, the Ni-rich cathodes suffer from some disadvantages such as high surface residual lithium because of its high affinity to react with atmospheric H_2O and O_2, poor structural stability at elevated voltages and

[a]*Department of Electronics and Communication Engineering, School of Engineering and Sciences, SRM University-AP, Amaravati 522240, Andhra Pradesh, India. E-mail: sujith.k@srmap.edu.in*

[b]*SRM-Amara Raja Center for Energy Storage Devices, SRM University-AP, Amaravati 522240, Andhra Pradesh, India*

[c]*National Water and Energy Center, United Arab Emirates University, Al Ain 15551, United Arab Emirates*

[d]*Department of Engineering, Amity University Dubai, United Arab Emirates*

[e]*Department of Chemistry, School of Engineering and Sciences, SRM University-AP, Amaravati 522240, Andhra Pradesh, India. E-mail: pardha.m@srmap.edu.in*

[f]*Department of Electronics and Communication Engineering, Amrita School of Engineering Amaravati, Amrita Vishwa Vidyapeetham, Andhra Pradesh, 522503, India*

[g]*Department of Smart Green Technology Engineering, Pukyong National University, 45, Yongso-ro, Nam-gu, Busan 48547, Republic of Korea*

[h]*Department of Nanotechnology Engineering, Pukyong National University, 45, Yongso-ro, Nam-gu, Busan 48547, Republic of Korea*

† Electronic supplementary information (ESI) available. See DOI: https://doi.org/10.1039/d4se01297f

temperatures, and poor thermal stability. Addressing these issues has been one of the main focuses of the research community and various strategies have been adopted such as elemental doping, surface coating, and tailoring microstructures.[10,11] There has been much research using these strategies to overcome the mentioned issues, but still, there is room to improve and the recent trend suggests that a single modification won't be enough to overcome the demand but dual-modification might be an answer to these defects.

Surface coating has been one of the best strategies that has been adopted to mitigate the above issues. Surface coating with materials like ZrO_2,[12] MgO,[13] TiO_2,[14] and Al_2O_3 (ref. 15) has been widely studied as a coating material for Ni-rich cathodes because of the ability to form a stable interface layer between the electrolyte and cathode material protecting from surface-side reactions. The presence of residual lithium along the surface of the cathode is one of the common issues and utilizing that to react with the coating materials is one of the important strategies to reduce the residual lithium. Lithium-ion conductors are chosen as an alternative for metal oxide coating, Ying *et al.* synthesised a Li_2O–B_2O_3 glass-coated $LiNi_{0.8}Co_{0.2}O_2$ cathode,[16] and Wang *et al.* reported a Li_2O–B_2O_3 glass-coated $LiNi_{0.5}Co_{0.2}Mn_{0.3}O_2$ cathode,[17] with enhanced high-voltage electrochemical performances and thermal stability. Chae *et al.* synthesised a Li_2O–$2B_2O_3$–glass-coated $LiNi_{0.5}Mn_{1.5}O_4$ cathode with remarkable electrochemical reversibility and stability at elevated temperatures.[18] Furthermore, Lin *et al.* showed that a glass-like LBO layer coated on the surface of the cathode materials through a simple mechanical mixing with H_3BO_3 exhibited high capacity and increased cycling performances.[19] These reports show that coating the cathode with boron-containing compounds will have a positive effect and enhance the electrochemical performance.

The structural stability at elevated voltages and temperatures is one of the major issues that prevails in Ni-rich cathodes. Several strategies to suppress the phase transitions at higher voltages and enhance the rate capability have been looked into so far and doping ions with strong metal–oxygen bonds is one of the sound strategies that has been used over the years to overcome these issues.[20,21] Mg^{2+} is an attractive dopant with high Mg–O bonding (394 kJ mol^{-1}) that can have a positive effect on the host structure. It acts as a "pillar" ion that restrains the Jahn–Teller distortion, thus ensuring structural stability during the charge/discharge process.[22] Moreover, Mg^{2+} occupies the Li sites preferentially to the Ni cations to compensate for lithium deficiency, thus suppressing the Ni^{2+}/Li^+ cation exchange in the formation of the layered structure. Theoretical calculations suggest that Mg^{2+} ions can be incorporated into Li sites within layered $LiMnO_2$ and Li_2MnO_3. This is because the energy difference between the Li-site and Mn-site doping is relatively small, making it possible for Mg^{2+} to occupy Li sites during high-temperature synthesis. Similar behaviour has been observed in Mg^{2+}-doped $LiNiO_2$ and $LiCoO_2$, where Mg^{2+} ions occupy both Li and transition metal (TM) sites. Additionally, in Mg^{2+}-doped $LiNiO_2$, Mg^{2+} ions in the TM layer can migrate into the Li layer during cycling. These findings indicate that Mg^{2+} can thermodynamically occupy Li sites in $LiMO_2$. However, no reports have shown selective Mg^{2+} doping exclusively at Li sites in $LiMO_2$.[23–25] Still, reports show that it positively affects electrochemical performance, which can thus be attributed to the material's higher electrochemical performance in this study.

High-energy density cathodes are of high requirement in the EV arena and to develop Ni-rich cathodes that can perform well at elevated voltages and temperatures is of utmost importance. The strategies suggested above can overcome the disadvantages to some extent but it is clear that a single modification alone is not enough. Thus, dual-modification of the cathodes has been studied recently to enhance the performance of the cathode at elevated voltages and temperatures. Kang *et al.* proposed a simple dual-modification by simultaneous Li_2SnO_3 surface coating and Sn^{4+} gradient doping. The proposed dual structural modifications could simultaneously address the interfacial instability and bulk structure degradation, thus enhancing the electrochemical performance of the NCM622 cathode.[26] In our previous work, we did a similar dual-modification by using ZrO_2 as a coating material and Zr^{4+} as a dopant, which enhanced the electrochemical performance due to the synergistic effect of ZrO_2 and Zr^{4+} in the NCM-622 cathode.[27] Even though the dual modification has enhanced the performance of the cathode, some problems persist while cycling at elevated voltages and temperatures; the structural irreversibility at higher voltage is an issue that needs to be addressed to achieve high-energy density cathodes. Furthermore, similar studies have shown the importance of dual and co-modification and their positive impact on Ni-rich cathodes. In this work, we have reported a $LiBO_2/B_2O_3$ hybrid coating layer that reacts with the residual lithium on the surface and Mg^{2+} doping into the host structure, which can be stable at elevated voltage (up to 4.5 V) and temperature (55 °C). This hybrid coating layer might be multi-functional with $LiBO_2$ as a Li-ion conductor. The amorphous B_2O_3 layer can protect the surface from HF attacks during high-voltage cycling. The hybrid coating layer formation can be explained using the reaction shown in eqn (1), where the formation of $LiBO_2$ removes the residual Li on the surface and the remaining H_3BO_3 transforms into B_2O_3 as shown in eqn (2).[28]

$$H_3BO_3 + LiOH \rightarrow LiBO_2 + H_2O \quad (1)$$

$$H_3BO_3 \rightarrow 1/2B_2O_3 + 3/2H_2O \quad (2)$$

The $LiBO_2/B_2O_3$ hybrid coating layer was prepared by a simple wet chemical coating technique and comprehensive investigations have been conducted to know how the hybrid coating layer helps in enhancing the performance of the cathode during the high voltage and temperature cycling and with the presence of Mg^{2+} as a dopant help in stabilizing the structure under harsh conditions. The cathode exhibited enhanced electrochemical performance and better structural reversibility than the bare and single-modified cathodes due to dual-modification where the surface is protected by the hybrid layer and the structural reversibility is ensured by the dopant (Scheme 1).

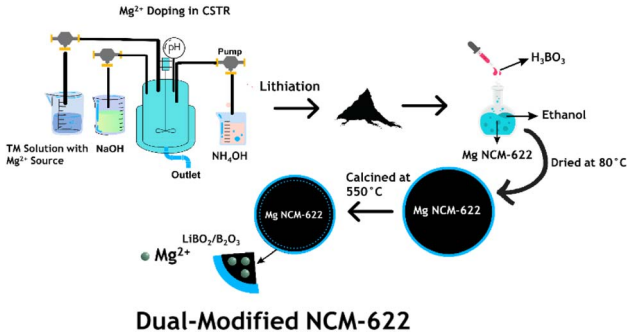

Scheme 1 Synthesis of Mg NCM-622 by using a CSTR and wet chemical coating of the $LiBO_2/B_2O_3$ layer on Mg NCM-622.

Experimental section

$LiBO_2/B_2O_3$ hybrid surface coating

Mg-NCM-622 was synthesised through a co-precipitation reaction by using a CSTR as previously reported.[29] The lithiated Mg-NCM-622 was added to an ethanol solution and stirred for a few minutes. Then, H_3BO_3 (boric acid) was used as a precursor for boron coating. It was added to the ethanol mixture and stirred under heating until it evaporated. Next, the dried mixture was calcined at 550 °C for 5 h under an O_2 atmosphere to achieve the $LiBO_2/B_2O_3$ coating.

Material characterization

X-ray diffraction (XRD) measurements were performed using an X-ray diffractometer (PANalytical Empyrean) with Cu-Kα radiation. The intensity data were recorded in the 2θ window of 10°–90° with a step size of 0.01. HighScore Plus software was used for the Rietveld refinements. The particle size was measured by using a Horiba LA-350 particle size analyzer. The morphology of the samples was analyzed by High Resolution-Scanning Electron Microscopy (HR-SEM Thermoscientific Apreo S) and High Resolution-Transmission Electron Microscopy (HR-TEM JEOL-JEM 2100) along with energy-dispersive X-ray spectroscopy (EDS) for determining the composition and elemental distribution. XPS analysis (ULVAC – PHI5000) was carried out to determine the oxidation states of Ni, Co, Mn, Mg, and B.

Electrochemical measurements

The cathode was fabricated by taking the active material, carbon black, and PVDF as a binder in the weight ratio of 90 : 5 : 5. The mixture was thoroughly mixed in a mortar and pestle and made into a slurry by adding *N*-methyl pyrrolidone (NMP) solution. The resulting slurry was cast onto a piece of aluminum foil using the doctor blade technique and dried at 80 °C overnight in a vacuum oven. The active material loading ratio was 7–9 mg cm^{-2}. The CR2032-type coin cells were used to analyze the electrochemical performance of the cathode and were assembled in a vacuum glove box filled with argon using Li foil as the reference/counter electrode, Celgard as the separator, and $LiPF_6$ dissolved in ethylene carbonate (EC), ethyl methyl carbonate (EMC) and diethyl carbonate (DEC) (1 : 1 : 1 volume) as the electrolyte solution. The assembled cells were cycled in the voltage ranges of 2.8–4.3 V and 2.8–4.5 V in a Neware battery tester at room temperature, and temperature studies were done at 55 °C with a temperature chamber interconnected with the battery tester.

Results and discussion

The crystal structures of pristine $LiNi_{0.6}Co_{0.2}Mn_{0.2}O_2$ (NCM-622), Mg– $Ni_{0.6}Co_{0.2}Mn_{0.2}O_2$ (Mg NCM-622), and BM- $Ni_{0.6}Co_{0.2}Mn_{0.2}O_2$ ($LiBO_2/B_2O_3$ Mg NCM-622) are explored by XRD, as presented in Fig. 1(a). The diffraction peak positions of all samples are similar and without excess impurity peaks, which matched well with the α-$NaFeO_2$ layered structure with the $R\bar{3}m$ space group. The distinct split between (006)/(012) and (018)/(110) means a well developed layered structure. Furthermore, the cation intermixing/disorder can be measured from the peak intensity ratio of $I_{(003)}/I_{(104)}$; the higher the ratio, the lower the intermixing degree of Li^+/Ni^{2+}. As a result, the values of the $I_{(003)}/I_{(104)}$ ratio of all samples are higher than 1.2 (Table 1), meaning that the materials have a well-ordered layered structure. From this, we can infer that the coating layer didn't affect the crystal structure and the boron compound reacted with the residual lithium on the surface of the cathode (LiOH & $LiCO_2$).[28,30,31] The refinement parameters given in Table 1 for all three samples indicate that the change in the lattice parameters is mainly due to the Mg^{2+} doping in the structure and may be due to the presence of little B^{3+} in the structure. This can also be verified using the magnified image of the (003) plane in the XRD shown in Fig. 1(b), where the peak shift can be seen towards a lower angle meaning an increase in the lattice parameter. The expansion of both the lattice parameters *a* and *c* with the Mg doping and boron coating can be seen in Table 1. The enlarged *c*-axis can be explained by the smaller Ni^{2+} (0.64 Å) ion replaced by the larger Mg^{2+} (0.72 Å) in the Li sites and *a* axis enlargement may be due to some amount of Mg present in the TM sites (Co^{3+} 0.545 Å, Mn^{4+} 0.53 Å, Ni^{3+} 0.56 Å). Due to the stronger bond of Mg–O than the Ni–O we can say that the increase in both the parameters is due to the presence of Mg in both the TM and Li

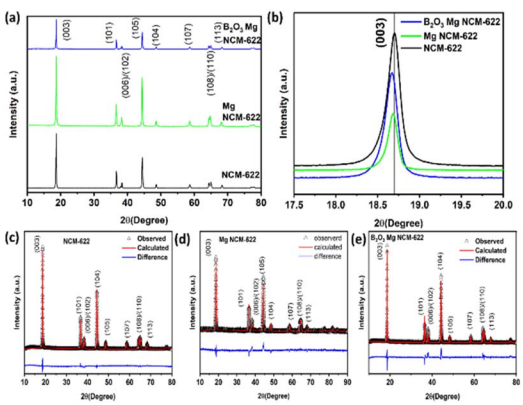

Fig. 1 (a) XRD pattern of the cathode materials, (b) magnified (003) plane image, and (c to e) Rietveld refinement images of the cathode materials.

Table 1 Rietveld refinement parameters for NCM, MNCM and BMNCM cathodes

Sample name	a (Å)	c (Å)	c/a	V (Å^3)	χ^2	I_{003}/I_{104}
NCM-622	2.8673	14.2184	4.958	101.23	1.98	1.556
Mg NCM-622	2.8698	14.2239	4.959	101.45	1.50	1.628
$LiBO_2/B_2O_3$ Mg NCM-622	2.8789	14.2244	4.940	102.66	2.66	1.695

sites. Moreover, the presence of Mg^{2+} ions in the Li slabs enhances the structural stability and improves the diffusion of Li^+ ions during cycling which can be seen in the electrochemical results.[22,32] HR-SEM analysis was done to analyse the morphologies of all the compounds and EDX elemental mapping was done to check the presence of all the elements in the synthesised compound. Fig. 2(a and b) show the HR-SEM and EDX elemental mapping of the bare and BM-NCM compounds. The cathode shows a spherical kind of morphology and the presence of all the elements has been verified by the elemental mapping. Similarly, the HR-TEM analysis was performed to check the presence of a coating layer along the surface of the modified cathode; Fig. 2(c) shows the presence of a coating layer of a thickness of around 1–2 nm along the surface and Fig. 2(d) shows well-ordered lattice fringes of around 0.474 nm which matches the (003) plane of the crystal lattice of the $R\bar{3}m$ space group. The deconvoluted XPS spectra of B_{1s}, Mg_{2p}, and Ni_{2p} are shown in Fig. 3 to check the surface chemistry of the cathodes. The peaks at 190.5 eV and 191.7 eV correspond to the $LiBO_2$ and B_2O_3 species in the B_{1s} spectra, and the Mg_{1s} spectra shows that the Mg is in the +2 oxidation state. The XPS peak of Co_{2p} and Mn_{2p} species shows the valences of +3 and +4, and the modified sample's Ni_{2p} peak shifted from lower binding energy to higher binding energy, indicating that the Mg^{2+} doping increases the Ni^{3+} on the surface than in the the bare sample. The presence of Ni^{3+} favours the reduction of Li^+/Ni^{2+} mixing, which is evident from the XRD results.[33]

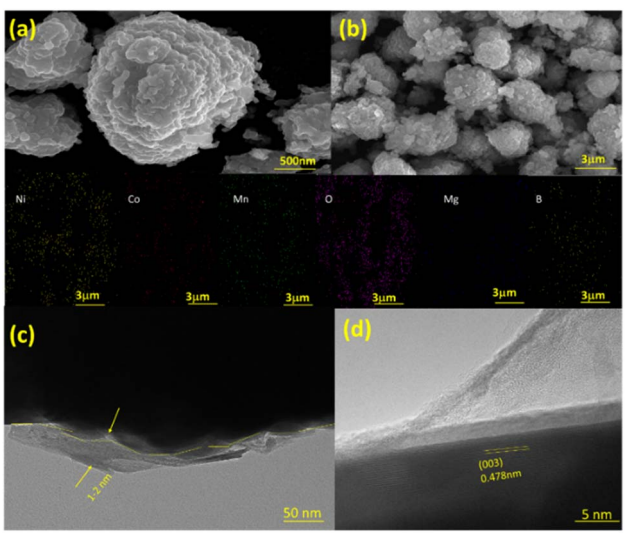

Fig. 2 (a & b) SEM and EDX images of NCM-622 and BM NCM-622. (c & d) HR-TEM images of BM NCM-622.

Electrochemical analysis

All the cathode materials were charged at a 0.1C rate to analyze the initial charge/discharge capacity (2.8 V to 4.3 V) as shown in Fig. 4(a). The BM-NCM cathode exhibited the highest capacity of 183.4 mA h g^{-1}, whereas the M-NCM cathode exhibited a capacity of 167.2 mA h g^{-1} and the bare material exhibited only 163.9 mA h g^{-1}. The higher initial discharge capacity of the BM-NCM cathode can be attributed to the presence of the $LiBO_2/B_2O_3$ hybrid coating layer which aids in suppressing the surface reaction and alleviating the electrode polarisation. The minimal change in the bare and M-NCM cathode capacity can be because of little Mg^{2+} ions occupying the Ni sites, meaning a higher percentage of doping will have a negative effect because of the electrochemically inactive Mg ions.[34,35] Fig. 4(c) shows the cycling stability of all the cathodes cycled at 1C rate (4.3 V) and the dual-modified cathode BM-NCM shows higher capacity retention of 85.8% even after 150 cycles, whereas the bare and M-NCM cathodes exhibited only 78.5% and 88% capacity retention, respectively, after 100 cycles. The higher capacity retention can be due to the presence of a $LiBO_2$ layer on the surface that protects the NCM cathode by restraining the formation of Li_2CO_3 or LiOH on the electrode surface, thus preventing erosion by acids produced from the electrolytes during cycling. The better cycling stability of the M-NCM

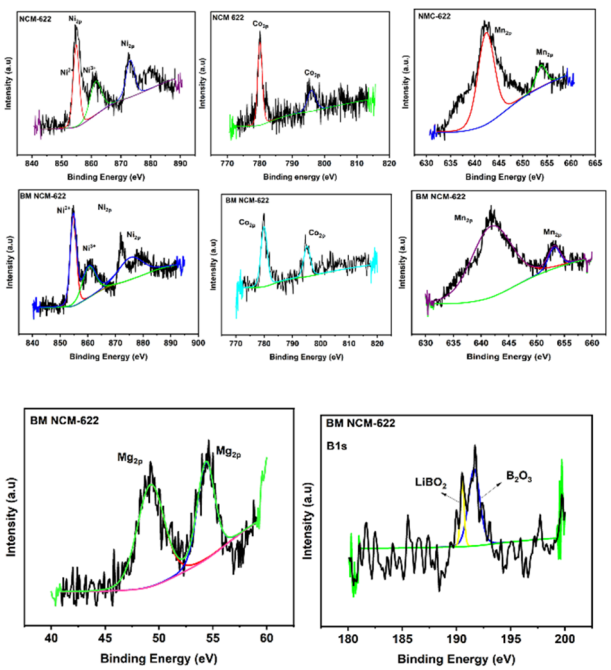

Fig. 3 XPS spectra of NCM-622 and BM NCM-622 cathode materials.

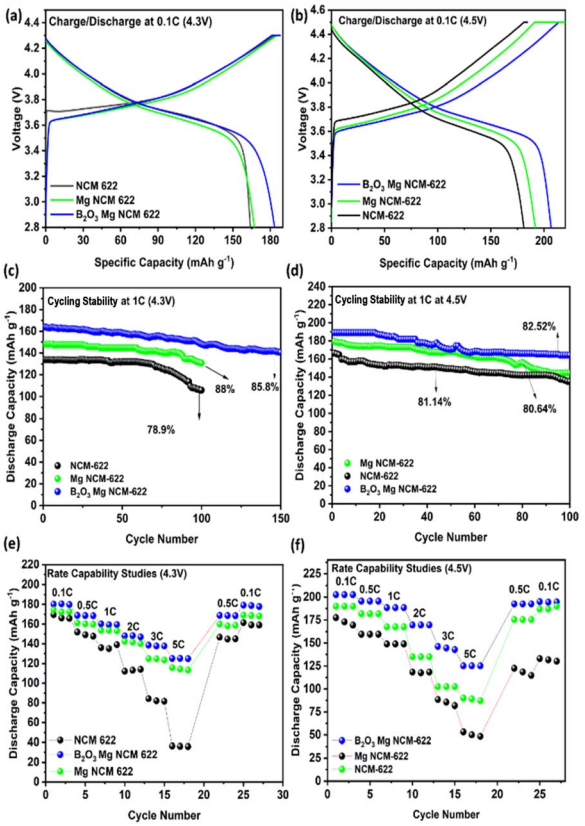

Fig. 4 (a & b) Initial charge/discharge graph of all three cathodes at 4.3 V and 4.5 V, (c & d) cycling study graphs of all the cathodes at 4.3 V and 4.5 V, and (e & f) rate capability studies for all the cathodes at 4.3 V & 4.5 V.

cathode than the bare material can be particularly due to the presence of Mg^{2+} ions in the host structure. The Mg^{2+} ions can act as a 'pillar' between the Li^+ and Ni^{2+} layers and the greater bonding strength of the Mg–O (394 kJ mol^{-1}) than the Ni–O (391.6 kJ mol^{-1}) enhances the structural stability of the M-NCM cathode.[36,37] The cathode, when subjected to dual modification, demonstrated superior electrochemical stability compared to other cathodes, indicating the positive impact of this dual-modification approach. The incorporation of a hybrid coating layer comprising $LiBO_2/B_2O_3$ effectively mitigates impedance by suppressing surface-side reactions, while the high ionic conductivity of LBO facilitates swift Li^+ transport during charge and discharge cycles. Additionally, the optimized presence of Mg^{2+} within the structure ensures unimpeded Li^+ diffusion by maintaining open Li^+ channels.[38,39] Furthermore, the rate capability studies for samples—bare, M-NCM, and BM-NCM—were analysed ranging from 0.1C to 5C as shown in Fig. 4(e). The BM-NCM cathode exhibited higher rate capability than the other cathodes by retaining 69.4% of its initial capacity even at a 5C rate. This can be mainly attributed to the presence of dual-modification on the BM-NCM cathodes; in addition, the $LiBO_2$ coating acts as a lithium-ion reservoir compensating for Li loss at high C-rates and it also facilitates fast Li-ion kinetics by creating a more favourable pathway for the Li-ion diffusion.[40] The BM-NCM cathode performed well even at a C-rate of 5C and retained 96.2% of its initial capacity, whereas the bare cathode failed at a higher C-rate of 5C by retaining only 74.9% of its initial capacity.

High-energy density lithium-ion batteries are very much the need of current demand, thus testing cathodes at high cut-off voltages is very important to determine their performance. Thus, all the cathodes were subjected to high voltage cycling at 4.5 V. Fig. 4(b) shows the initial charge/discharge capacity graph of the bare, M-NCM, and BM-NCM cathodes cycled at 0.1C rate (4.5 V). The dual-modified BM-NCM cathode exhibited a higher discharge capacity of 206.6 mA h g^{-1} than the M-NCM and bare cathodes (191.7 and 180.8 mA h g^{-1}, respectively). When the upper cut-off voltage increases we can see a slight increase in the capacity of all the cathodes but this significant increase in the capacity of the BM-NCM can again be attributed to the presence of the $LiBO_2/B_2O_3$ hybrid coating layer. Fig. 4(d) shows the cycling stability graph at a 1C rate cycled at the upper cut-off voltage of 4.5 V; here we can see that the BM-NCM cathode shows better cycling stability by retaining 82.52% of its original capacity, whereas the bare and M-NCM cathodes were only able to retain 67.04 and 80.64%, respectively, of their initial capacity after 100 cycles. Furthermore, rate capability analysis was done for all the cathodes at 4.5 V as shown in Fig. 4(f); surprisingly even at the elevated voltage the BM-NCM cathode exhibited superior rate capability even when cycled at 5C. When cycled back to 0.1C after cycling at 7C, the BM-NCM cathode recovered 88% of its initial capacity compared to the bare one which recovered only 50% of its initial capacity. This can mainly be due to the presence of a $LiBO_2/B_2O_3$ hybrid coating layer on the surface of the cathode. The decomposition of the organic electrolyte at higher voltages and temperatures can cause the formation of HF which can react with the cathode's surface and end in corrosion of the cathode material, which results in serious deterioration of the capacity and stability of the cathode. The presence of a hybrid $LiBO_2/B_2O_3$ coating layer on the surface protects the cathode from the HF attack and alleviates the development of cracks along the grain boundaries causing the penetration of the electrolyte into the cathode, which will eventually pulverise the cathode.[41,42]

Additionally, to know the best performance of the cathode, it was subjected to cycling under harsh conditions say at 55 °C until 4.3 V and 4.5 V as shown, respectively, in Fig. 5 & 6. At elevated temperatures, the cycling stability deteriorates soon due to the breakdown of the electrolyte causing unwanted surface side reactions which also result in the formation of a thick and resistive Solid Electrolyte Interface layer (SEI) and the structural change that the Ni-rich cathodes undergo at elevated temperatures may lead to the breakdown of the cathode.[27,43] As shown in Fig. 5, the bare cathode after cycling at 1C (4.3 V) suffered capacity degradation and retained only 49.9% of its initial capacity whereas the M-NCM and BM-NCM cathodes showed better electrochemical stability and retained 83.78% and 88.16%, respectively, of their initial capacity even after 100 cycles. Furthermore, when cycled at a higher voltage (4.5 V) at 55 °C as shown in Fig. 6, the capacity and the stability deterioration are even more visible with the bare cathode only retaining 35.01% of its initial capacity whereas the dual-

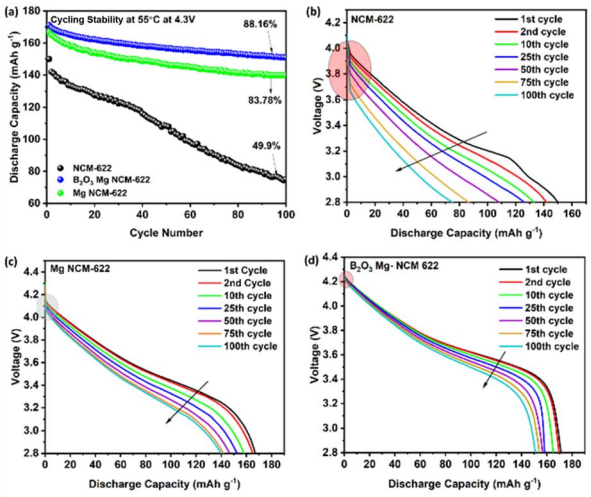

Fig. 5 (a) Cycling stability studies upon cycling at 1C at 55 °C (2.8 to 4.3 V) and (b to d) average discharge voltage graphs for all the cathodes.

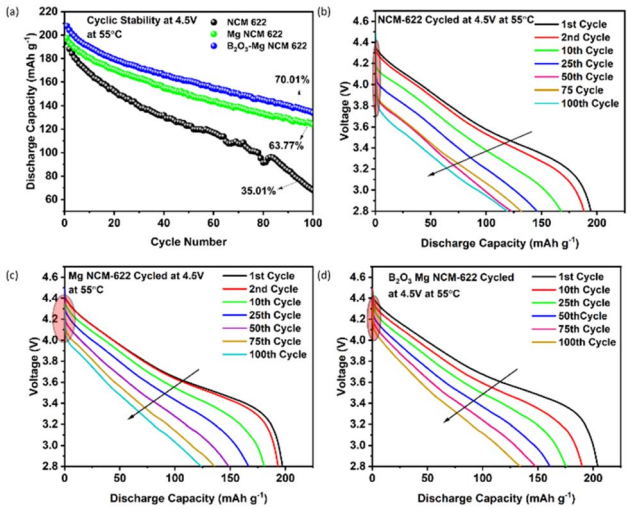

Fig. 6 (a) Cycling stability studies upon cycling at 1C at 55 °C (2.8 to 4.5 V) and (b to d) average discharge voltage graphs for all the cathodes.

modified cathode retained 70% of its initial capacity even after 100 cycles. Fig. 5(b–d) show the discharge curves of NCM, M-NCM and BM-NCM at different cycles (2nd, 25th, 50th, 75th, and 100th) at 1C and 2.8–4.3 V (55 °C), and Fig. 6(b–d) show the discharge curves of NCM, M-NCM and BM-NCM at different cycles (2nd, 25th, 50th, 75th, and 100th) at 1C and 2.8–4.5 V (55 °C). The average discharge voltage of NCM drops sharply from 3.51 to 3.28 V (4.3 V) and 3.59 to 3.24 (4.5 V), and the potential decay is 0.23 V (4.3 V) & 0.35 V (4.5 V), respectively. In contrast, the potential decay of BM-NCM is only 0.07 V (from 3.67 to 3.60 V (4.3 V)) & 0.18 V (from 3.72 to 3.54 V (4.5 V)), which illustrates that dual-modification can reduce the polarisation of LIBs.[44] As shown in the *ex situ* analysis of cycled electrodes after 100 cycles at 4.5 V (55 °C) in Fig. S1,† the (003) peak is absent in NCM622, while in MNCM, it appears less sharp compared to BM-NCM. This suggests that dual modification effectively preserves the crystal structure after prolonged cycling at high temperatures and voltages. This can further be validated in the dQ/dV analysis shown in Fig. 7. The difference in the oxidation peak is caused by the structural change from the layered to rock-salt phase during the high voltage charge/discharge process. The narrow gap and small oxidation peak difference shown in BM-NCM (Fig. 7(c)) of 0.134 V show that the dual modification can alleviate the structural change and reduce the polarisation in LIBs.[45,46] As shown in Fig. 8, the B_2O_3 coating fends off the HF attack during the high voltage and temperature cycling. At the same time, the $LiBO_2$ coating facilitates fast Li-ion movement, paving the way for enhanced performance of the cathode and Mg as a dopant in the structure, helping in the better electrochemical performance of the cathode. Furthermore, the EIS analysis done for the cathodes cycled at 2.8–4.3 V is shown Fig. S2.† In the spectrum, a larger semicircle at medium frequency represents the charge transfer resistance (R_{ct}) at the electrode–electrolyte interface, while the oblique line at low frequency corresponds to the Warburg resistance, indicating

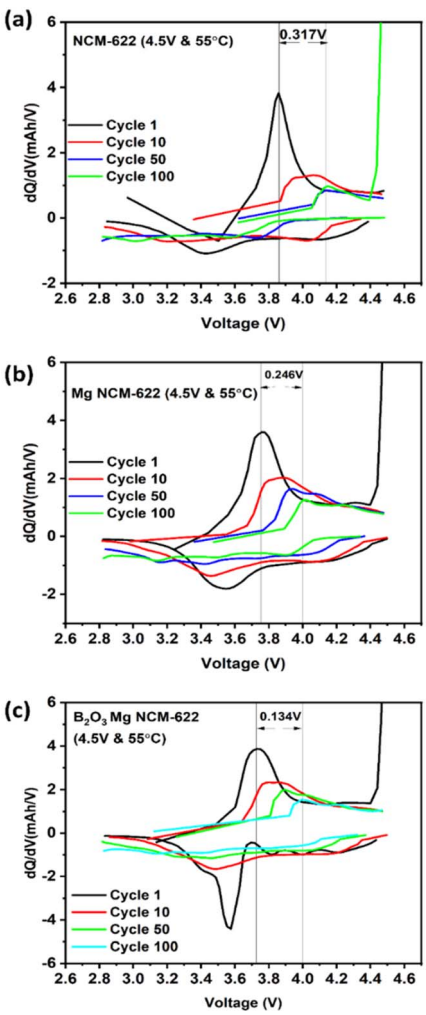

Fig. 7 dQ/dV analysis for the cathodes at 1C cycled at 2.8 to 4.5 V (55 °C): (a) NCM, (b) M NCM, and (c) BM NCM.

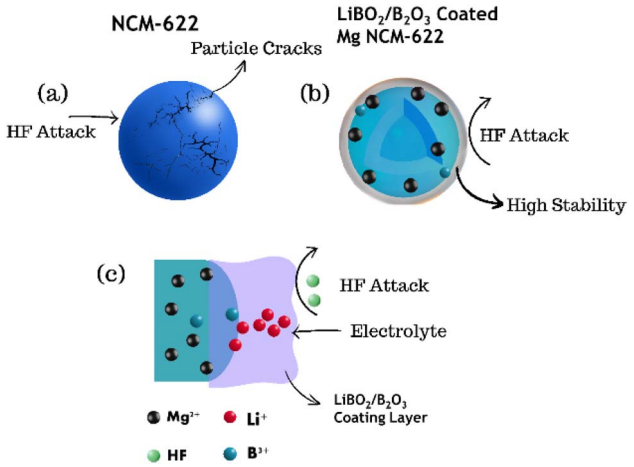

Fig. 8 (a) Bare NCM-622, (b) dual-modified NCM-622 & (c) mechanism of surface protection using the hybrid layer.

solid-state lithium-ion diffusion within the electrode bulk. Notably, the charge transfer resistance of the boron-modified (BMNCM) electrode is lower than that of pristine NCM622. Moreover, the interfacial resistance of both electrodes increases with cycling. However, the significantly reduced interfacial resistance of the BM electrode during cycling suggests that the coated layer on the active material surface effectively mitigates SEI film thickening. This protective layer minimizes side reactions with the electrolyte, thereby preventing excessive interfacial resistance build-up.

Conclusion

The dual-modification of Mg-NCM-622 with a $LiBO_2/B_2O_3$ hybrid coating layer was successfully done by a wet chemical coating process. The formation of $LiBO_2$ consumed the residual lithium present on the surface of the cathode and that helps in facilitating the fast Li kinetics and the formation of amorphous B_2O_3 due to the decomposition of remaining H_3BO_3 after its reaction with residual Li impurities, making the cathode resistant to electrolyte induced corrosion. Moreover, the presence of Mg^{2+} ions in the host structure enhances the structural stability. It alleviates the large anisotropic lattice distortions at elevated voltages and temperatures due to the proposed "pillar effect". The dual modification significantly improved the electrochemical performance of the BM NCM cathode by improving the cycling stability and rate capability. The proposed cathode showed a capacity retention of 82.5% even at 4.5 V even after 100 cycles. Furthermore, the high-temperature cycling of the modified cathode exhibited enhanced performance proving that the presence of the hybrid coating layer facilitates fast Li kinetics and Mg doping ensures the structural reversibility making this dual modification a viable strategy for future applications.

Data availability

The data supporting this article have been included as part of the ESI.†

Conflicts of interest

There are no conflicts to declare.

Acknowledgements

The authors greatly acknowledge the financial support and infrastructure facilities provided by SRM University-AP through the SEED Research Grant (SRMAP/URG/SEED/2024-25/038), DST-SERB Start-up Research Grant (SRG/2019/000194), the Government of India, and Amara Raja Energy and Mobility Limited.

References

1 C.-S. Wang, G. A. Covic and O. H. Stielau, *IEEE Trans. Power Electron.*, 2004, **19**, 995–1002.
2 J. M. Tarascon and M. Armand, *Nature*, 2001, **414**, 359–367.
3 M. Armand and J. M. Tarascon, *Nature*, 2008, **451**, 652–657.
4 A. Manthiram, *J. Phys. Chem. Lett.*, 2011, **2**, 176–184.
5 A. Manthiram, *Nat. Commun.*, 2020, **11**, 1–9.
6 M. Kotal, S. Jakhar, S. Roy and H. K. Sharma, *J. Energy Storage*, 2022, **47**, 103534.
7 N. Nitta, F. Wu, J. T. Lee and G. Yushin, *Mater. Today*, 2015, **18**, 252–264.
8 J. Kim, H. Lee, H. Cha, M. Yoon, M. Park and J. Cho, *Adv. Energy Mater.*, 2018, **8**, 1702028.
9 N. Y. Park, H. H. Ryu, G. T. Park, T. C. Noh and Y. K. Sun, *Adv. Energy Mater.*, 2021, **11**, 03767.
10 U. H. Kim, J. H. Park, A. Aishova, R. M. Ribas, R. S. Monteiro, K. J. Griffith, C. S. Yoon and Y. K. Sun, *Adv. Energy Mater.*, 2021, **11**, 00884.
11 H. H. Ryu, B. Namkoong, J. H. Kim, I. Belharouak, C. S. Yoon and Y. K. Sun, *ACS Energy Lett.*, 2021, **6**, 2726–2734.
12 M. Khalili Azar, M. A. Razmjoo Khollari, M. Esmaeili, E. Heidari, S. M. Hosseini-Hosseinabad, R. Siavash Moakhar, A. Dolati and S. Ramakrishna, *ACS Appl. Energy Mater.*, 2021, **4**, 934–945.
13 M. R. Laskar, D. H. K. Jackson, S. Xu, R. J. Hamers, D. Morgan and T. F. Kuech, *ACS Appl. Mater. Interfaces*, 2017, **9**, 11231–11239.
14 X. Xi, Y. Fan, Y. Liu, Z. Chen, J. Zou and S. Zhu, *J. Alloys Compd.*, 2021, **872**, 159664.
15 R. S. Negi, E. Celik, R. Pan, R. Stäglich, J. Senker and M. T. Elm, *ACS Appl. Energy Mater.*, 2021, **4**, 3369–3380.
16 J. Ying, C. Wan and C. Jiang, *J. Power Sources*, 2001, **102**, 162–166.
17 D. Wang, X. Li, Z. Wang, H. Guo, X. Chen, X. Zheng, Y. Xu and J. Ru, *Electrochim. Acta*, 2015, **174**, 1225–1233.
18 J. S. Chae, S.-B. Yoon, W.-S. Yoon, Y.-M. Kang, S.-M. Park, J.-W. Lee and K. C. Roh, *J. Alloys Compd.*, 2014, **601**, 217–222.
19 J. Lin and L. Fang, *Energy Technol.*, 2021, **9**, 00721.
20 Y. S. Byeon, W. Lee, S. Park, D. Kim, J. Jung, M. Park and W. Yoon, *Small Sci.*, 2024, **4**, 2400165.
21 B. Chu, L. You, G. Li, T. Huang and A. Yu, *ACS Appl. Mater. Interfaces*, 2021, **13**, 7308–7316.

22 S. A. S. Paniyarasi, J. A. Sneha, S. Padmaja, M. P. Selvi, S. Sinthika and R. N. Elizabeth, *Nano-Struct. Nano-Objects*, 2020, **24**, 100559.
23 Y. Zhang, H. Li, J. Liu, J. Zhang, F. Cheng and J. Chen, *J. Mater. Chem. A*, 2019, **7**, 20958–20964.
24 K. Min, S. W. Seo, Y. Y. Song, H. S. Lee and E. Cho, *Phys. Chem. Chem. Phys.*, 2017, **19**, 1762–1769.
25 D. Buchholz, C. Vaalma, L. G. Chagas and S. Passerini, *J. Power Sources*, 2015, **282**, 581–585.
26 C.-Y. Kang, S. Oh, T. Y. Shim and S.-H. Lee, *Electron. Mater. Lett.*, 2023, **19**, 374–383.
27 P. Venkatachalam, K. K. Duru, M. Rangarajan, S. Sangaraju, P. S. Maram and S. Kalluri, *J. Mater. Sci.*, 2024, **59**, 548–562.
28 Y. Su, L. Li, L. Chen, L. Wang, Y. Lu, Q. Zhang, L. Bao and F. Wu, *ACS Appl. Energy Mater.*, 2022, **5**, 2231–2241.
29 P. Venkatachalam, K. K. Duru, M. Rangarajan, S. Sangaraju, P. S. Maram and S. Kalluri, *J. Mater. Sci.*, 2024, **59**, 548–562.
30 G. Yang, L. Huang, J. Song, G. Cong, X. Zhang, Y. Huang, J. Wang, Y. Wang, X. Gao and L. Geng, *ACS Appl. Mater. Interfaces*, 2023, **15**, 1592–1600.
31 T. Sattar, S. H. Lee, S. J. Sim, B. S. Jin and H. S. Kim, *Int. J. Hydrogen Energy*, 2020, **45**, 19567–19576.
32 S. Jamil, R. Yu, Q. Wang, M. Fasehullah, Y. Huang, Z. Yang, X. Yang and X. Wang, *J. Power Sources*, 2020, **473**(15), 228597.
33 N. Zhang, Y. Li and Y. Qiao, *J. Mater. Sci. Technol.*, 2021, **89**, 167–178.
34 Q. Xie, W. Li and A. Manthiram, *Chem. Mater.*, 2019, **31**, 938–946.
35 H. Yu, H. Zhu, Z. Yang, M. Liu, H. Jiang and C. Li, *Chem. Eng. J.*, 2021, **421**, 128625.
36 K. Min, S. W. Seo, Y. Y. Song, H. S. Lee and E. Cho, *Phys. Chem. Chem. Phys.*, 2017, **19**, 1762–1769.
37 J. Y. Hwang, T. Y. Yu and Y. K. Sun, *J. Mater. Chem. A*, 2018, **6**, 16854–16862.
38 S. Gao, B. Shi, J. Liu, L. Wang, C. Zhou, C. Guo, J. Zhang and W. Li, *ACS Sustain. Chem. Eng.*, 2021, **9**, 5322–5333.
39 X. D. Zhang, J. L. Shi, J. Y. Liang, L. P. Wang, Y. X. Yin, K. C. Jiang and Y. G. Guo, *J. Power Sources*, 2019, **426**, 242–249.
40 V.-C. Ho, M. Hong, T. B. T. Hoang, T. T. Mai and J. Mun, *Mater. Today Energy*, 2023, **35**, 101329.
41 X. Zeng, T. Jian, Y. Lu, L. Yang, W. Ma, Y. Yang, J. Zhu, C. Huang, S. Dai and X. Xi, *ACS Sustain. Chem. Eng.*, 2020, **8**, 6293–6304.
42 H. Zhang, J. Xu and J. Zhang, *Front. Mater.*, 2019, **6**, 309.
43 P. Venkatachalam, K. K. Duru, M. Rangarajan, S. Sangaraju, P. S. Maram and S. Kalluri, *J. Solid State Electrochem.*, 2024, **28**, 3509–3515.
44 F. Schipper, M. Dixit, D. Kovacheva, M. Talianker, O. Haik, J. Grinblat, E. M. Erickson, C. Ghanty, D. T. Major, B. Markovsky and D. Aurbach, *J. Mater. Chem. A*, 2016, **4**, 16073–16084.
45 L. Xu, F. Zhou, J. Kong, Z. Chen and K. Chen, *Ionics*, 2018, **24**, 2261–2273.
46 L. Tian, H. Yuan, Q. Shao, S. D. A. Zaidi, C. Wang and J. Chen, *Ionics*, 2020, **26**, 4937–4948.